Design and Optimization of an In-wheel Unequal Stator Teeth Motor

Lassaad Zaaraoui*‡, Ali Mansouri*, Nadia Smairi**

*Laboratory of Technology, Energy, and Innovative Materials, Faculty of Sciences of Gafsa, University of Gafsa, Tunisia

**COSMOS Laboratory, National School of Computer Sciences, University of Manouba, Tunisia

(lassaad.zaaraoui@gmail.com, ali.mansouri@isetgf.rnu.tn, nadia.smairi@gmail.com)

‡Corresponding Author; Lassaad Zaaraoui, Laboratory of Technology, Energy, and Innovative Materials, Faculty of Sciences of Gafsa, University of Gafsa, Tunisia, Tel: +216 23 319 476, lassaad.zaaraoui@gmail.com

Received: 07.01.2022 Accepted: 06.02.2022

Abstract- Recently, many researches have been focusing on finding new machine topologies that maximize the efficiency and minimize the mass of in-wheel motors for electric vehicles. This paper presents the design and the optimization of a new in-wheel motor for electric vehicles. This was achieved by proposing a new topology including unequal stator teeth. The design of the machine was performed with an analytical model that considers the slotting effect and the saturation when calculating the air gap flux density. The main purpose of the optimization process is to determine the optimal machine geometric dimensions. This optimization was performed according to three objective functions while respecting a set of constraints. The first objective function is to maximize the machine's efficiency, the second is to minimize the mass, and the third is to minimize the torque ripple. In this regard, four multiobjective optimization algorithms were employed: two of them belong to the particle swarm optimization family, and the others are genetic algorithms. An optimized machine design was chosen and analyzed using finite element analysis (FEA). The comparison of FEA and optimization results showed a good agreement between both of them, and proves the validity of the proposed design.

Keywords In-wheel motor; permanent magnet machine; unequal stator teeth; multiobjective optimization; finite element analysis.

Abbreviations

emf	Electromotive force
EV	Electric vehicles
FEA	Finite element analysis
NSGA-II	Nondominated Sorting Genetic Algorithm II
NSGA-III	Nondominated Sorting Genetic Algorithm III
OMOPSO	Multi-Objective Particle Swarm Optimizer
PMSM	Permanent magnet synchronous machine
SMPSO	Speed-constrained Multi-Objective PSO
UNET	Unequal teeth width

Symbols

A_{cu}	Area of a copper winding
B_m	Average air gap flux density
B_r	Remanent flux density of magnet
B_{ry}	Rotor yoke flux density
B_{sy}	Stator yoke flux density
B_{st1}	Widest stator tooth flux density
B_{st2}	Narrowest stator tooth flux density
b_{ts1}	1st stator teeth width (wider)
b_{ts2}	2nd stator teeth width (narrower)
$B_{\delta 1}$	Amplitude of air gap flux density
D_{rext}	Rotor outer diameter
D_{rint}	Rotor inner diameter
D_{sint}	Stator inner diameter
E_1	Fundamental rms value of the induced emf
$\hat{E}_i$	i^{th} harmonic of the induced emf
f	Frequency of the emf
h_m	Magnet height
h_s	Stator slot height
I_1	Fundamental rms stator current
J_s	Current density
K_c	Carter's coefficient
k_{eddy}	Eddy current coefficient
k_{exc}	Excess eddy current loss coefficient
k_{hyst}	Hysteresis coefficient

k_j	Stacking factor
k_s	Saturation factor
k_δ	Air gap coefficient
$k_{\omega 1}$	Winding factor
l	Axial machine length
l_{act}	Equivalent axial length of the stator core
l_{turn}	Length of one copper turn
N_c	Number of turns per phase
p	Pairs poles number
P_{co}	Copper losses
P_e	rms electromagnetic power
P_{iron}	Iron losses
P_{ry}	Iron loss in the rotor yoke
P_{sy}	Iron loss in the stator yoke
P_{st1}	Iron loss in the wider stator teeth
P_{st2}	Iron loss in the narrower stator teeth
Q_s	Slots number
T_e	Mean torque of this machine
T_{rip}	Torque ripple

Greek Symbols

α	Half pole angle
α_m	Magnet pole coverage coefficient
α_p	Pole arc coefficient
β	Angular displacement, Steintmetz constant
δ	Air gap length
δ_e	Effective air gap length
η	Machine efficiency
μ_r	Relative permeability of magnet
ρ	Copper resistivity
σ	Leakage flux factor
τ_f	Distance between magnets
ω_r	Rotor speed

1. Introduction

Anxious to offer innovative mobility solutions that act with energy efficiency and environmental protection, electric vehicles (EVs) are becoming more and more attractive for road transport [1-3]. They offer the following advantages: absence of urban pollution, limited noise, reduced operating cost, and longer life [4-5].

The basic technology of electric vehicles is motor drives. More accurately, permanent magnet synchronous machines (PMSMs) are currently the most attractive motors for propulsion of electric vehicles [6]. Their main characteristics are: high power density, high efficiency, light weight, compact structure and flexibility in control [7,8].

Several criteria make it possible to distinguish the different topologies of PMSMs, namely: the direction of the magnetic flux, the rotor position, the magnets location and the distribution of the windings. Thus, the machine structure depends on the specifications of the industrial application in question. As far as we are concerned, the PMSM is intended for in-wheel direct-drive application.

One of the greatest advantages of in-wheel electric motors is the fact that the clutch, drive shafts, and suspension become unnecessary, which makes it possible to reduce the weight and the interior of the vehicle [9,11]. Furthermore, in-wheel motors provide the ability to transmit power directly from the motor to the wheel and deliver torque to each wheel independently, hence increasing the motor's efficiency and improving the vehicle's stability [11].

Despite of these upsides of in-wheel motors, they also have disadvantages that impede them from being employed in production vehicles, such as the restricted in-wheel's space and the increased wheel's weight which lead to decreased comfort and road holding abilities [12].

To remedy these disadvantageous, several works are concerned with the design and the evaluation of the in-wheel permanent magnet motors. Indeed, in [13], a design and performance analysis of an in-wheel outer rotor PMSM intended for electric vehicles was presented. The main objective of this work is to achieve the optimal design while maximizing the torque density and minimizing the torque ripple. The studied machine was tested using finite element method. The results showed that the optimized parameters improved the machine's performance.

In [14], a multiphysics analysis including electromagnetic, mechanical, and thermal aspects, of an axial flux in-wheel motor for a solar-powered electric vehicle was presented. Moreover, a prototype of the studied machine was fabricated and tested. The multiphysics analysis results were compared with the prototype test results, and the comparison showed that the proposed axial flux in-wheel motor can be an efficient and simple option for electric vehicles.

An analysis and design of an axial flux permanent magnet in-wheel motor for electric vehicle was introduced in [15]. The authors proposed a novel analytical method combined with a finite element analysis to reduce the cost and time factors in the development of the studied machine. Furthermore, the authors showed that the novel analytical method combined with the numerical method can consider the nonlinear characteristics of the studied machine such as the magnetic saturation and the slot opening effects. Finally, it was showed that the proposed analysis and design method can improve efficiency and torque density, and can also be applied to a variety of electrical machine topologies.

A surface-mounted permanent magnet in-wheel motor for electric vehicles was synthetically optimized in [16]. During the optimization procedure, all the design requirements are taken into account as objective functions and optimization constraints. Moreover, a genetic algorithm (NSGA-II) was used to search the optimal design of the studied machine and the finite element method was employed to analyze the designed motor. The results showed that the best performance of the studied machine can be achieved with the optimum design which is verified by FEA.

In [17], an in-wheel outer rotor permanent magnet reluctance motor was designed for an electric vehicle. The authors proposed a new rotor topology to improve the machine's performance. The designed motor was tested using finite element method and the simulation results showed that the motor can achieve the maximum torque and minimum torque ripple by improving the rotor geometry.

The present survey is devoted to design and optimize a new in-wheel motor. After the selection of the machine topology, an analytical model which deals with the electromagnetic properties is developed. For the optimization procedure, four multiobjective optimization algorithms are applied. The results of the employed algorithms are compared and analyzed. Finally, the optimization results are compared with finite element analysis (FEA) results.

2. Selection of the in-Wheel Motor Topology

For the in-wheel motor drive, radial flux permanent magnets machines are widely used. These machines remain by far the easiest to implement and the cheapest [18]. The outer-rotor machine topology is highly desirable for in-wheel motor in EVs [7] [18]. Indeed, the outer rotor corresponding to a large radial diameter which can accommodate a large number of poles, hence increasing the torque density. Moreover, the outer-rotor structure facilitates the direct coupling with the rim of the wheel, hence improving the mechanical integrity. Another advantage of this topology is the reduction of the total machine's mass [18]. In addition, this machine adopts the surface-mounted permanent magnets rotor. This structure brings on the benefits of simplicity and economy [7]. Moreover, centrifugal forces exert pressure on the magnets glued on the inner surface of the rotor, which makes their detachment more difficult and gives good mechanical strength to the machine.

The main novelty in this topology is that the stator adopts unequal teeth width (UNET) without tooth tips. According to [19-21], this structure has the best performance compared to other stator structures. Indeed, this stator composition makes it possible to increase the average electromagnetic torque and the electromotive force, to improve the fault tolerance ability [19], and to reduce copper losses, torque ripple and motor mass [20].

For the windings type, the stator of the machine adopts single-layer concentrated windings. In fact, the use of concentrated windings reduces both copper losses and the machine's weight [22]. Other advantages of this windings configuration obviously reside in the high power density, the simplicity of manufacture, and the low cost [19] [22-23].

Choosing the number of layers depends mainly upon the stator production method. For a structure of unequal teeth, single layer windings are more preferable than double layer windings. Indeed, this configuration makes it possible to reduce the torque ripple and to increase the average torque compared to a machine with equal teeth with single or double layer windings [24].

After selecting single-layer concentrated windings as a winding type, the next step is to choose the poles/slots numbers. This combination must be chosen with care in order to maximize the winding factor and then maximize the electromagnetic torque. To do this, the difference between the poles number (2p) and the slots number (Q_s) must be the smallest integer. The reasonable relation between these two numbers is $Q_s = 2p \pm 2$. Our proposed proportion is 18 slots and 16 poles. This proportion provides excellent performance, limits the motor's vibration and noise, and produces a balanced electromagnetic torque [21]. It should also be noted that assembling the windings in the wider teeth of the UNET stator increases the winding factor and flux linkage of the windings [19].

To conclude, the new topology of the in-wheel motor drive is a 3-phase, 18-slots, 16-poles, surface-mounted PMSM with an outer-rotor and unequal stator teeth without tooth tips. A two-dimensional layout of the studied topology is shown in Fig.1.

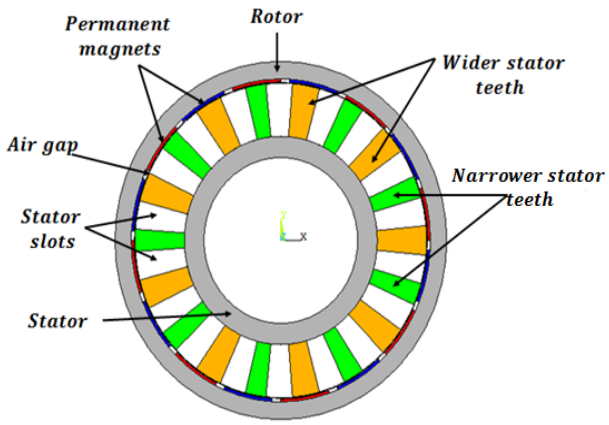

Fig. 1. Two-dimensional layout of machine.

3. Analytical Model

After determining the machine's topology, the poles/slots numbers, and the associated windings, the next step in the machine design and optimization is to develop the analytical model, which makes it feasible to describe the machine by equations and in turn making the system more explicit.

3.1. Machine characteristics

The sizing of the machine is based on certain main parameters. These parameters are given in Table 1 with their ranges of values. It is worth noting that the rotor's outer diameter (D_{rext}) is fixed at 255 mm.

Table 1. Main parameters of machine

Main parameters	Symbol	Bounds
Air gap length	δ	[1 ; 2]
Rotor inner diameter	D_{rint}	[225 ; 230]
Magnet height	h_m	[2 ; 4]
1st Stator teeth width (wider)	b_{ts1}	[21 ; 27]
2nd Stator teeth width (narrower)	b_{ts2}	[15 ; 17]
Stator slot height	h_s	[30 ; 40]
Axial machine length	l	[70 ; 85]
Half pole angle	α	[19 ; 21]
Stator inner diameter	D_{sint}	[115 ; 122]

3.2. Magnetic proprieties

In this section, we define the main magnetic characteristics of the machine by calculating the flux densities in all machine parts.

3.2.1 Magnetic proprieties

In this analytical model, the calculation of the average air gap flux density (B_m) is done by considering the slotting effect and saturation of iron material. The consideration of these two phenomena is done respectively by the air gap coefficient, the leakage flux factor and the saturation factor [25]. They are represented by the following equations:

The air gap coefficient k_δ [26]:

$$k_\delta = \frac{k_c\left(h_m + \delta\right) - h_m}{\delta} \tag{1}$$

Where K_c is the Carter's coefficient. It's given by:

$$k_C = \frac{\tau_s}{\tau_s - \sigma_\delta b_{ss1}} \tag{2}$$

$$\sigma_\delta = \frac{2}{\pi}\left\{\arctan\left(\frac{b_{ss1}}{2\left(\delta + h_m\right)}\right) - \frac{\delta + h_m}{b_{ss1}}\ln\left[1 + \left(\frac{b_{ss1}}{2\left(\delta + h_m\right)}\right)^2\right]\right\} \tag{3}$$

The leakage flux factor σ [28]:

$$\sigma = 1 + \frac{\delta_e\left[\frac{4\delta_e}{\tau_f + \delta_e} + \frac{4\delta_e}{b_{ss1} + 2\delta_e} + \frac{2}{\pi}\ln\left(1 + \frac{\pi\delta_e}{h_m}\right)\right]}{\tau_m + 2\delta_e} + \frac{\frac{2\delta_e}{3\pi}\tau_m \ln\left(1 + \frac{3\pi\delta_e}{2h_m}\right)}{\left(\tau_m + 2\delta_e\right)\left(l + 2\delta_e\right)} \tag{4}$$

Where δ_e and τ_f are respectively the effective air gap length, and the distance between magnets. They are given by the following equations:

$$\delta_e = k_c\delta \tag{5}$$

$$\tau_f = \tau_p - \tau_m \tag{6}$$

The stator permeability, and thus the air gap flux density are vastly affected by the saturation of stator iron material. The saturation factor k_s has a range of values between 1.05 and 1.3 [28].

After defining the factors of the slotting effect and saturation, the average air gap flux density can be defined by the following equation [25]:

$$B_m = B_r\frac{h_m}{\mu_r k_\delta k_s\delta + A\sigma h_m} \tag{7}$$

Where B_r is the remanent flux density of magnet, μ_r is the relative permeability of magnet, and the coefficient A is defined by the following expression:

$$A = \frac{D_{sext}\left(l + 2\delta\right)\alpha_m}{lD_{r\,\mathrm{int}}\alpha_p} \tag{8}$$

Where α_m is the magnet pole coverage coefficient, and α_p is the pole arc coefficient which is equal to 0.7 [28].

Based on equation (7), the fundamental amplitude of air gap flux density ($B_{\delta 1}$) can be written [18]:

$$B_{\delta 1} = \frac{4}{\pi}B_m \sin\left(\frac{\alpha_m\pi}{2}\right) \tag{9}$$

3.2.2 Flux densities in ferromagnetic parts

The flux densities in the rotor yoke (B_{ry}) and the stator yoke (B_{sy}) are calculated by the following equations [12]:

$$B_{ry} = \frac{B_m\tau_m}{2h_{ry}k_j} \tag{10}$$

$$B_{sy} = \frac{B_m\tau_m}{2h_{sy}k_j} \tag{11}$$

Where k_j is the stacking factor of the lamination.

The current linkage of the end windings creates a fringing magnetic flux which also participates in the output torque production [29]. For this reason, the equivalent axial length of the stator core ought to be increased in order to include the air gap [30]:

$$l_{act} = l + 2\delta \tag{12}$$

In this regard, the flux densities in the widest teeth (B_{st1}) and narrowest teeth (B_{st2}) are computed respectively by the following equations [8] [25] [30]:

$$B_{st1} = \frac{B_m\tau_s l_{act}}{b_{ts1}k_j l} \tag{13}$$

$$B_{st2} = \frac{B_m\tau_s l_{act}}{b_{ts2}k_j l} \tag{14}$$

3.3. Electric proprieties

This section deals with the electrical modeling of the studied machine. Indeed, the equations of the induced electromotive force, the electromagnetic power, the electromagnetic torque, the copper and iron losses are presented in this section.

3.3.1 Induced electromotive force

The fundamental rms value of the induced emf of a phase is given by [18]:

$$E_1 = 4.44fN_c k_{w1}B_{\delta 1}\frac{\left(D_{sext} + \delta\right)}{p}l_{act} \tag{15}$$

Where f is the frequency of the emf, N_c is the number of turns per phase, and $k_{\omega 1}$ is the winding factor.

3.3.2 Electromagnetic power

Consider a balanced three-phase winding, the rms electromagnetic power developed by the machine is given by the following equation:

$$P_e = 3E_1 I_1 \sin(\beta) \tag{16}$$

Where I_1 is the fundamental rms stator current, and β is the angular displacement between the fields produced by the magnet and the stator current.

3.3.3 Electromagnetic torque

The developed mean torque of this machine (T_e) is expressed by the ratio of the electromagnetic power (P_e) to the rotor speed (ω_r). After substitution, we obtain:

$$T_e = \frac{P_e}{\omega_r} = \frac{3}{\sqrt{2}} N_c k_{w1} B_{\delta 1} (D_{sext} + \delta) l_{act} I_1 \sin(\beta) \tag{17}$$

3.3.4 Copper losses

The copper losses (P_{co}) for a three-phase machine are given by the following equation [31]:

$$P_{co} = 3{I_1}^2 \frac{\rho(120°).l_{turn}}{A_{cu}} N_c \tag{18}$$

Where ρ (120°) is the copper resistivity at 120°, lturn is the length of one copper turn, A_{cu} is the area of a copper winding, and N_c is the number of turns per phase.

3.3.5 Iron losses

The iron losses can be obtained using the following equation [18] [30]:

$$P_{iron} = k_{hyst} B^{\beta} f + k_{eddy} (Bf)^2 + 8.67 k_{exc} (Bf)^{1.5} \tag{19}$$

Where k_{hyst} is the hysteresis coefficient, B is the induction, β is the Steintmetz constant, k_{eddy} is the eddy current coefficient, k_{exc} is the excess eddy current loss coefficient.

To calculate the iron losses in the rotor yoke (P_{ry}), the stator yoke (P_{sy}), the wider stator teeth (P_{st1}) and the narrower stator teeth (P_{st2}), it suffices to replace the value of (B) by the corresponding induction while multiplying the whole equation by the volume of the corresponding part.

4. Used Optimization Techniques

We present in this section four state-of-the-art multiobjective optimization algorithms adopted to find the optimal geometry of the in-wheel motor.

4.1. Multi-Objective Particle Swarm Optimizer (OMOPSO)

OMOPSO algorithm [32] is based on communication mechanisms within a population of particles. Each particle has a small memory that allows it to memorize the best position already encountered by its neighbors, its best position, and its current position. The movement of a particle in the search space is partly influenced by its neighborhood, which is made up of all the particles that have an information link with it and by its experience [8].

Furthermore, OMOPSO algorithm is an improved approach of multiobjective PSO algorithms that makes it doable to carry out a multiobjective optimization gleaned from the Pareto dominance principle. Assuredly, it uses an external archive to conserve the non-dominated solutions that are found during the optimization process. It adopts the crowding distance mechanism to guide the leaders selection and prevent the explosion of the external archive. After dividing the swarm into three sub-swarms of the same size, it applies a different mutation technique to each one of them. In fact, this mutation mechanism aims to maintain the diversity in the Pareto front and to prevent the swarm stagnation in local optima [8]. Finally, this algorithm adopts the ε-dominance concept to define the number of final solutions in the archive.

4.2. Speed-constrained Multi-Objective PSO (SMPSO)

The authors have presented in [33] the SMPSO algorithm, which is based on the OMOPSO algorithm. They present a mechanism for limiting the speed of particles movement in the OMOPSO algorithm. Indeed, following an experimental study of the OMOPSO behaviour, the authors found that the majority of particles move to their extreme values continuously, so they do not contribute to research. The authors then proposed a speed constriction mechanism to prevent its irregular variations. This mechanism increases the performance of the algorithm as it allows particles to move along different regions of the search space. Moreover, SMPSO algorithm applies a polynomial mutation on 15% of the swarm's particles in order to maintain the diversity.

4.3. Nondominated Sorting Genetic Algorithm II (NSGA-II)

Similar to the earliest evolutionary algorithms, the NSGA-II algorithm [34] is inspired by the mechanisms of natural evolution. It relies based on three major operations, which are: selection, recombination, and mutation. Additionally, this approach is built on several classification fronts, where each of them corresponds to a group of individuals having the same degree of Pareto dominance. Furthermore, the conservation of new solutions of each generation is done without the use of an external archive, which allows the convergence acceleration towards the optimal solutions, and the increase of algorithm's performance. Besides, NSGA-II adopts the crowding distance mechanism to guide the selection process. This mechanism helps to maintain the diversity of solutions and to reduce the computational complexity of the algorithm.

4.4. Nondominated Sorting Genetic Algorithm III (NSGA-III)

Due to the drawbacks encountered in many-objective optimization (i.e. dealing with a problem that has more than

3 objective functions), the NSGA-III algorithm [35], which is gleaned from the NSGA-II algorithm, has been proposed to find a set of non-dominated and well diversified solutions. Indeed, the optimization of a many-objective problem increases the proportion of non-dominated solutions of a generation, hence slowing down the search process. Moreover, the implementation of a traditional operator for preserving diversity (such as crowding distance) becomes a computationally expensive operation. In addition, a large population size is required to represent a large-dimensional optimal Pareto front, which causes difficulties for the decision-maker in choosing a preferred solution.

To remedy the aforementioned problems, the authors of the NSGA-III significantly change the selection operator used in the NSGA-II algorithm. On top of that, they replace the crowding distance mechanism with a strategy that places a set of reference points on a normalized hyper-plane to find a set of broadly distributed optimal Pareto solutions. The NSGA-III algorithm has been applied to 3-objective to 15-objective test problems, and it has shown that it is able to effectively find a well-diversified and well-converged set of non-dominated solutions in all of these problems [35].

5. Formulation of the Optimization Problem

Once the equations of the machine sizing, the magnetic and electric behaviours have been computed, a model is needed to transform the design problem into an optimization problem, where we define the design variables, the objective functions, as well as the various constraints.

5.1. Design Variables

To proceed with the optimal sizing of the machine, there are 9 machine parameters to be optimized. These parameters are given in Table 1.

5.2. Objective functions

In this work, the optimization process focuses on three objectives functions. Indeed, these objectives are concerned with increasing the machine efficiency, reducing its mass, and minimizing torque ripple. They are expressed by the following equations:

$$objective\_function1 = \text{minimize}\left(1-\eta\right) \tag{20}$$

Where η is the machine efficiency, and given by:

$$\eta = \frac{P_{out}}{P_{out} + P_{co} + P_{ry} + P_{st} + P_{st1} + P_{st2}} \tag{21}$$

$$objective\_function2 = \text{minimize}\left(mass\right) \tag{22}$$

Where mass is the total machine mass.

$$objective\_function3 = \text{minimize}\left(T_{rip}\right) \tag{23}$$

Where T_{rip} is the torque ripple, and it can be formulated as:

$$T_{rip} = 2\frac{\sqrt{\left(\hat{E}_7 - \hat{E}_5\right)^2 - \left(\hat{E}_{13} - \hat{E}_{11}\right)^2 - \left(\hat{E}_{19} - \hat{E}_{17}\right)^2 - \left(\hat{E}_{25} - \hat{E}_{23}\right)^2}}{\hat{E}_1} \tag{24}$$

Where $\hat{E}_i$ is the i^{th} harmonic of the induced emf.

5.3. Optimization constraints

The sizing of the geometric parameters of the machine imposes a set of constraints to be respected. In our optimization process, we applied two types of constraints. The first type is used to define the search space. It aims to limit the design parameters by defining their values range. These intervals are given in Table 1. Further, the second type serves to define the space of achievable solutions. These constraints are imposed in order to avoid the magnetic saturation. They are presented in Table 2.

Table 2. Magnetic constraints (Tesla [T])

Variables	Constraints
The fundamental air gap flux density	$0.85 \leq B_{\delta 1} \leq 0.95$
The rotor yoke flux density	$B_{ry} \leq 1.6$
The stator yoke flux density	$B_{sy} \leq 1.8$
The widest stator tooth flux density	$B_{st1} \leq 2$
The narrowest stator tooth flux density	$B_{st2} \leq 2$

6. Optimization Results

In this section, we present the optimization results of the applied algorithms. For the computation, we have employed the "Eclipse" software and the "jMetal framework" which is for the multiobjective optimization algorithms in object-oriented Java. First, we expose the generated Pareto front of each algorithm. Then, we present the most important optimal geometry of each algorithm. Finally, we investigate the effectiveness of the optimization results using the finite element analysis.

6.1. Pareto fronts

The Pareto fronts generated by the applied algorithms are illustrated in Fig. 2, Fig. 3, Fig. 4, and Fig. 5.

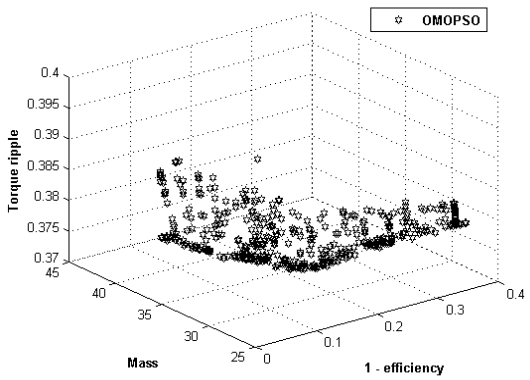

Fig. 2. OMOPSO Pareto front.

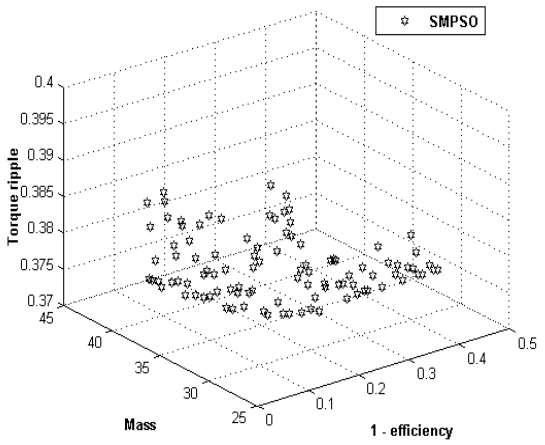

Fig. 3. SMPSO Pareto front.

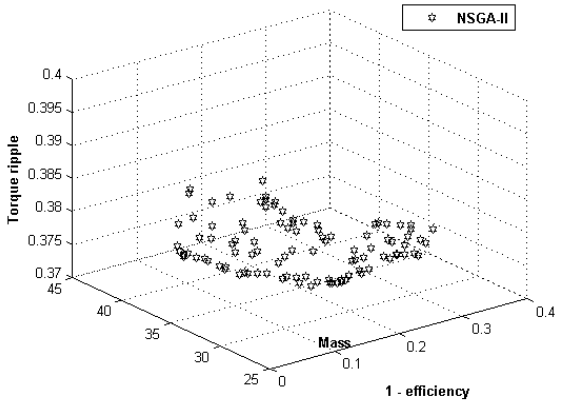

Fig. 4. NSGA-II Pareto front.

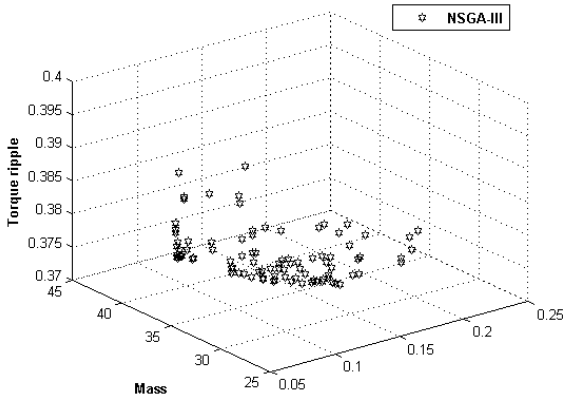

Fig. 5. NSGA-III Pareto front.

Despite the contradiction of the objective functions, the Pareto fronts show that the optimization algorithms are able to generate well-diversified optimal solutions, and the designer can then select the points that meet the design requirements. However, regarding the number of solutions generated, the OMOPSO algorithm shows that it can produce a richer front of solutions than the other algorithms, since it generates more than 400 optimal solutions at each execution. SMPSO and NSGA-II algorithms are very competitive as they engender 100 solutions at each execution. For the NSGA-III algorithm, it can only bring about 90 to 100 solutions at each execution.

6.2. Optimal geometries of algorithms

The most important optimization results of the machine geometry, with respect to the three objective functions, are demonstrated in the Table 3.

Table 3. Optimization algorithms results

	OMOPSO	**SMPSO**	**NSGA-II**	**NSGA-III**
δ	1	1	1	1
D_{rint}	229.88	230	225.25	229.98
h_m	2.03	2	2.03	2
b_{ts1}	21.29	21.09	21.09	21
b_{ts2}	16.79	16	16.82	15.66
h_s	35.93	33.83	33.71	35.72
l	78.35	78.25	81.76	77.79
α	19.11	19.21	19	19
D_{sint}	115	116.12	121.93	121.90
Efficiency	88.24%	88.30%	87.74%	88.07
Mass	31.85	31.58	31.73	30.83
T_{rip}	0.378	0.382	0.375	0.375
Execution time (s)	6.538	5.780	6.896	6.685

The results show that SMPSO is the fastest algorithm, and NSGA-II is the slowest algorithm. Moreover, SMPSO has the best result regarding the machine efficiency, but also the highest torque ripple value. The best machine mass is obtained by means of the NSGA-III algorithm.

6.3. Finite element analysis

To prove the efficiency of the optimization procedure, the optimal machine was analyzed using the finite element method. For the analytical calculations, we have employed the "Ansys engineering simulation software" and we have used the optimization results to define all dimensions of the machine. For this comparison, we have used the optimization results of the SMPSO algorithm as it provides the best result concerning the machine's efficiency and a good result regarding the mass. The meshed study domain and the considered boundary conditions have been shown in Fig. 6. The results are demonstrated in Table 4, and Fig. 7.

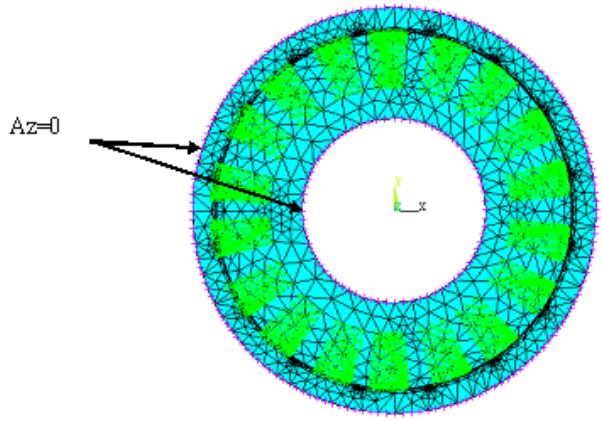

Fig. 6. Meshed study domain.

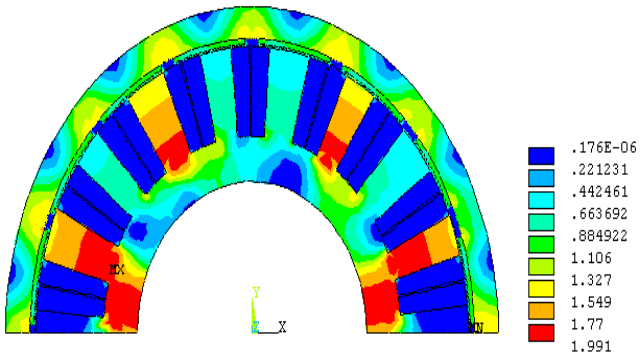

Fig. 7. 2-D flux density plot (J_s= 6.05 10^6).

Table 4. Optimization algorithms results

Flux densities	Optimization results	FEA results	Error
$B_{\delta 1}$	0.87	0.97	10.3 %
B_{ry}	1.12	1.15	2.6 %
B_{sy}	0.69	0.73	5.4 %
B_{st1}	1.40	1.46	4.1 %
B_{st2}	1.84	1.95	5.6 %

According to these results, the analytical calculations agree very well with the FEA results, which makes the proposed optimization procedure a valuable tool for the design and optimization of permanent magnet motors, particularly for electric vehicles.

7. Conclusion

This paper proposed the design and the optimization of a new in-wheel motor for electric vehicle application. The machine topology is a radial flux, surface-mounted permanent magnet motor, with an outer-rotor and concentrated windings. The main novelty in this topology is that the stator adopts unequal teeth width (UNET) without tooth tips. To describe the electromagnetic proprieties of the machine, the analytical model was developed. The calculation of the air gap flux density was made by considering the slotting effect and saturation of the iron material.

The design was carried out using four multiobjective algorithms, and the optimization procedure was developed according to three objective functions, which are the maximization of the machine efficiency, the minimization of the mass, and the minimization of the torque ripple, while respecting a set of mechanical and magnetic constraints.

From the optimization results, it was shown that the applied algorithms can generate good Pareto fronts. The execution times of the algorithms are acceptable, and the optimization results are suitable for the optimization of the in-wheel motor. The designer can then select the solution that satisfies the design requirements.

In order to verify the efficiency of the optimization procedure, the analytical calculations were compared to the finite element simulation results. The analytical results agree very well with the FEA results, which makes the proposed optimization procedure a valuable tool for the design and optimization of permanent magnet motors, particularly the in-wheel motors for electric vehicles.

References

[1] M. Akil, E. Dokur, R. Bayindir, "Impact of Electric Vehicle Charging Profiles in Data-Driven Framework on Distribution Network," 9th International Conference on Smart Grid (icSmartGrid), Setubal, Portugal, 2021.

[2] M. Brenna, M. Longo, D. Zaninelli, R. Miceli, F. Viola, "CO2 reduction exploiting RES for EV charging," IEEE International Conference on Renewable Energy Research and Applications (ICRERA), Birmingham, UK, 2016.

[3] T. HARIGHI, B. BAYINDIR, E. Hossain, "Overviewing Quality of Electric Vehicle Charging Station's Service Evaluation," International Journal of Smart Grid - ijSmartGrid, Vol. 2, No. 1, pp. 40-48, 2018.

[4] L. Noel, G. Z. Rubens, J. Kester, and B. K. Sovacool, "Beyond emissions and economics: Rethinking the co-benefits of electric vehicles (EVs) and vehicle-to-grid (V2G)," Transport Policy, vol. 71, pp. 130-137, 2018.

[5] T. Sakagami, Y. Shimizu, H. Kitano, "Exchangeable batteries for micro EVs and renewable energy," IEEE 6th International Conference on Renewable Energy Research and Applications (ICRERA), San Diego, CA, USA, 2017.

[6] H. Turker, "Design optimization ofan interior permanent magnet synchronous machine (IPMSM) for electric vehicle application," IEEE International Conference on Renewable Energy Research and Applications (ICRERA), Birmingham, UK, 2016.

[7] K. T. Chau, Electric Vehicle Machines and Drives: Design, Analysis and Application. Wiley-IEEE Press, 2015.

[8] L. Zaaraoui and A. Mansouri, Conception optimale d'un moteur-roue destiné à un véhicule électrique. Editions universitaires européennes, 2019.

[9] R. Vos, "Influence of in-wheel motors on the ride comfort of electric vehicles," M. S. thesis, Eindhoven University of Technology, 2010.

[10] M. Andriollo, G. Bettanini, G. Martinelli, A. Morini, S. Stellin, and A. Tortella, "In-wheel permanent magnet motors for public transport application". 5th Int. Conf. on Electric Power Systems, High Voltages, Electric Machines, Tenerife, Spain, pp.156-164, 2005.

[11] F. Tahami, R. Kazemi, and S. Farhanghi, "A novel driver assist stability system for all-wheel-drive electric vehicles", IEEE Transactions on Vehicular Technology, vol. 52, pp. 683-692, 2003.

[12] Ö. Bingül, "Fuzzy logic based multi-objective optimization of active suspension system of 4x4 in-wheel motor driven electrical vehicle", Doctoral dissertation, Bursa Uludag University, Turkey, 2021.

[13] M. Y. Bdewi, A. M. Mohammed and M. M. Ezzaldean, "Design and Performance Analysis of Permanent Magnet Synchronous Motor for Electric Vehicles Application," Engineering and Technology Journal, Vol. 39, Part A, No. 03, pp. 394-406, 2021.

[14] T. Li, Y. Zhang, Y. Liang, Q. Ai, H. Dou, "Multiphysics analysis of an axial-flux in-wheel motor with an amorphous alloy stator", IEEE Access, vol. 8, pp. 27414-27425, 2020.

[15] B. O. Tak, J. S. Ro, "Analysis and design of an axial flux permanent magnet motor for in-wheel system using a novel analytical method combined with a numerical method", IEEE Access, vol. 8, pp. 203994-204011, 2020.

[16] X. Chen, H. Shu, Y. Song, "Synthetically optimal design of a direct-drive surface-mounted permanent magnet in-wheel motor", IEEJ Transactions on Electrical and Electronic Engineering, Vol. 15(5), pp. 652-657, 2020.

[17] A. Bozkurt, A. F. Baba, Y. Oner, "Design of Outer-Rotor Permanent-Magnet-Assisted Synchronous Reluctance Motor for Electric Vehicles", Energies , 14, 3739, 2021.

[18] A. Mansouri, "Conception et optimisation multi-objectifs d'un moteur à aimants permanents destiné pour un véhicule électrique," Habilitation universitaire, Génie électrique. Université de Gafsa, Tunisia, 2016.

[19] G. J. Li, Z. Q. Zhu, M. Foster, and D. Stone, "Comparative Studies of Modular and Unequal Tooth PM Machines Either With or Without Tooth Tips," IEEE Transactions on Magnetics, vol. 50, 2014.

[20] Y. Fan, S. Chen, C. Tan, and M. Cheng, "Design and investigation of a new outer-rotor IPM motor for EV and HEV in-wheel propulsion", 19th International Conference on Electrical Machines and Systems (ICEMS), Chiba, Japan, 2016.

[21] J. Xia, T. Dong, C. Wang, and J. Zhao, "Low speed high torque PMSM design based on unequal teeth structure", Proc. of the 2008 International Conference on Electrical Machines and Systems, Wuhan, China, 2008.

[22] Y. Choe , S. Oh, S. Ham, I. Jang, S. Cho, J. Lee, and K. Ko, "Comparison of concentrated and distributed winding in an IPMSM for vehicle traction", Proc. of the 2nd International Conference on Advances in Energy Engineering (ICAEE), Vol. 14, pp. 1368-1373, 2012.

[23] D. Martinez, "Design of a permanent magnet synchronous machine with non-overlapping concentrated windings for the shell eco marathon urban prototype," M. S. thesis, Royal Institute of Technology, Stockholm, 2012.

[24] S. P. Cheng and C. C. Hwang, "Design of high-performance spindle motors with single-layer concentrated windings and unequal tooth widths," IEEE Transactions on Magnetics, vol. 43, pp. 802-804, 2007.

[25] Y. L. Feng and C. N. Zhang, "Analytical calculation for predicting the air gap flux density in surface-mounted permanent magnet synchronous machine", Journal of Electrical Engineering and Technology, vol. 12, pp.769-777, 2017.

[26] T. Renyuan, Modern Permanent Magnet Machines. China Mechanical Press, Beijing, China, 2012.

[27] B. Liuxin, S. Wang, and Y. Xia, "Calculation of leakage permeance in a surface-mounted permanent magnet machine," Journal of Tsinghua University, vol. 50, pp. 525-528, 2010.

[28] C. He and T. Wu, "Permanent magnet brushless DC motor and mechanical structure design for the electric impact wrench system," Energies 2018, 11, 1360.

[29] P. Ponomarev, "Tooth-coil permanent magnet synchronous machine design for special applications," Doctoral thesis, Lappeenranta University of Technology, 2013.

[30] A. Mansouri, N. Smairi, and H. Trabelsi, "Multi-objective optimization of an in-wheel electric vehicle motor," International Journal of Applied Electromagnetics and Mechanics, vol. 50, pp. 449-465, 2016.

[31] T. D. Strous, "Design of a permanent magnet radial flux concentrated coil generator for a range extender application," M.S. thesis, Delft University of Technology, 2010.

[32] M.R. Sierra and C. Coello, "Improving PSO-based Multi-Objective Optimization using Crowding, Mutation and e –Dominance", Proc. of the 3rd International Conference on Evolutionary Multi-Criterion Optimization, Mexico, 2005.

[33] A. J. Nebro, J. J. Durillo, J. G. Nieto, C. A. Coelle, F. Luna, and E. Alba,, "SMPSO: A New PSO-based Metaheuristic for Multi-objective Optimization", Proc. of the 2009 IEEE Symposium on Computational Intelligence in Multi-criteria Decision-Making, pp. 66-73, 2009.

[34] K. Deb, A. Pratap, S. Agarwal, and T. Meyarivan, "A fast and elitist multiobjective genetic algorithm:NSGA-II," IEEE Transactions on Evolutionary Computation, vol. 6, pp. 182-197, 2002.

[35] K. Deb and H. Jain, "An Evolutionary Many-Objective Optimization Algorithm Using Reference-point Based Non-dominated Sorting Approach, Part I: Solving Problems with Box Constraints," IEEE Transactions on Evolutionary Computation, vol. 18, pp. 577-601, 2014.